Fukui I, Kihara K.					
Yamamoto M, Takeuchi K, Shimoji M, Maniwa T, Isaka M, Nakagawa K, Ohde Y, Kondo H, Nakajima T.	Small non-mucinous bronchioloalveolar carcinoma with anaplastic lymphoma kinase immunoreactivity: A novel ALK fusion gene?	Cancer Sci	103	390-392	2012
Kimura H, Nakajima T, Takeuchi K, Soda M, Mano H, Iizasa T, Matsui Y, Yoshino M, Shingyoji M, Itakura M, Itami M, Ikebe D, Yokoi S, Kageyama H, Ohira M, Nakagawara A.	ALK fusion gene positive lung cancer and 3 cases treated with an inhibitor for ALK kinase activity.	Lung Cancer	75	66-72	2012
Takahashi S, Iwase T, Kohno N, Ishikawa T, Taguchi T, Takahashi M, Horiguchi J, Nakamura S, Hozumi Y, Fukunaga M, Noguchi S.	Efficacy of zoledronic acid in postmenopausal Japanese women with early breast cancer receiving adjuvant letrozole: 12-month results.	Breast Cancer Res Treat.		in press	2012
Suzuki K, Terui Y, Nakano K, Nara E, Nasu K, Ueda K, Nishimura N, Mishima Y, Sakajiri S, Yokoyama M, Takahashi S, Hatake K.	High thymidine kinase activity is a strong predictive factor for poor prognosis in PTCLs treated by CHOP.	Leuk Lymphoma.	53(5)	849-54.	2012
Saad F, Brown JE, Van Poznak C, Ibrahim T, Stemmer SM, Stopeck AT, Diel IJ, Takahashi S, Shore N, Henry DH, Barrios CH, Facon T, Senecal F, Fizazi K, Zhou L, Daniels A, Carrière P, Dansey R.	Incidence, risk factors, and outcomes of osteonecrosis of the jaw: integrated analysis from three blinded active-controlled phase III trials in cancer patients with bone metastases.	Ann Oncol.	23(5)	1341-7.	2012
Sugawara S, Togashi Y, Kuroda N, Sakata S, Hatano S, Asaka R, Yuasa T, Yonese J, Kitagawa M, Mano H, Ishikawa Y, Takeuchi K.	Identification of ALK fusions in renal cancer: Large-scale immunohistochemical screening by intercalated antibody-enhanced polymer method.	Cancer		in press	
Maita S, Yuasa T, Tsuchiya N, Mitobe M, Narita S, Horikawa Y, Hatake K, Fukui I, Kimura S, Maekawa T, Habuchi T.	Antitumor effect of sunitinib against skeletal metastatic renal cell carcinoma through inhibition of osteoclast function.	Int J Cancer	130	677-84.	2012
Yuasa T, Tsuchiya N, Horikawa Y, Narita S, Inoue T, Urakami S, Yamamoto S, Yonese J, Takahashi S, Hatake K, Fukui I. Habuchi T.	Clinical Efficacy and Prognostic Factors for Overall Survival in Japanese Patients with Metastatic Renal Cell Cancer Treated with Sunitinib.	BJU int.		(in press).	

Yuji Mishima1, Yasuhito Terui1, Yuko Mishima, Ryoko Kuniyoshi1, Satoshi Matsusaka Mariko Mikuniya1, Kiyotsugu Kojima and Kiyohiko Hatake.	High reproducible ADCC analysis revealed a competitive relation between ADCC and CDC and differences between FcγRIIIa polymorphism.	Int. Immunol.	(in press)	doi: 10.1093/intimm/dxs048 First published online: March 21,	2012

IV. 研究成果の刊行物・別刷

Identification of CD20 C-Terminal Deletion Mutations Associated with Loss of CD20 Expression in Non-Hodgkin's Lymphoma

Yasuhito Terui,[1,3,4] Yuji Mishima,[3,4] Natsuhiko Sugimura,[4] Kiyotsugu Kojima,[4] Takuma Sakurai,[5] Yuko Mishima,[1,3] Ryoko Kuniyoshi,[3,4] Akiko Taniyama,[3,4] Masahiro Yokoyama,[1] Sakura Sakajiri,[1,3] Kengo Takeuchi,[2] Chie Watanabe,[1] Shunji Takahashi,[1,3] Yoshinori Ito,[1,3] and Kiyohiko Hatake[1,3,4]

Abstract

Purpose: Rituximab is commonly incorporated into CD20-positive B-cell lymphoma therapy to improve response and prognosis. With increasing use, resistance to rituximab is a continuing concern, but CD20 mutation as a cause of resistance has not previously been reported.

Experimental Design: Freshly collected lymphoma cells from 50 patients with previously untreated or relapsed/resistant non-Hodgkin's B-cell lymphomas (diffuse large B cell, $n = 22$; follicular, $n = 7$; mucosa associated lymphoid tissue, $n = 16$; chronic lymphocytic leukemia, $n = 2$; small lymphocytic lymphoma, $n = 1$; lymphoplasmacytic, $n = 1$; mantle cell lymphoma, $n = 1$) were assessed for CD20 expression by flow cytometry, and *CD20* gene sequencing was done on extracted DNA.

Results: CD20 mutations were found in 11 (22.0%) of 50 patients and could be grouped as C-terminal deletion (8.0%), early termination (10.0%), and extracellular domain (2.0%) or transmembrane domain (2.0%) mutations. The mean fluorescence intensity of CD20 on fresh lymphoma cells was significantly lower for the C-terminal deletion mutation [3.26; 95% confidence interval (95% CI), 0.09-6.89] compared with wild type (30.8; 95% CI, 22.4-39.2; $P < 0.05$). In contrast, early termination mutations did not show significant differences in CD20 expression compared with wild type (19.5; 95% CI, 10.7-28.4; $P > 0.05$).

Conclusions: It is possible that C-terminal deletion mutations of CD20 may be related to relapse/resistance after rituximab therapy. These mutations should be examined in patients showing progression of disease after partial remission.

Therapeutic monoclonal antibodies have been developed against cancer cells, such as malignant lymphoma, breast, and colorectal cancers, including rituximab (Mabthera/Rituxan; ref. 1), trastuzumab (Herceptin; ref. 2), and bevacizumab (Avastin; ref. 3), respectively. The rituximab target antigen is the B-cell membrane differentiation antigen CD20, and rituximab has emerged as a useful tool for adjunct cancer therapy (4). Although CHOP (cyclophosphamide, doxorubicin, vincristine, and prednisone/prednisolone) therapy leads to median overall survival rates of only 60%, addition of rituximab improves rates by ~20% (5).

With the need to determine standard first-, second-, and subsequent-line combination therapies using rituximab (6, 7), relapse/resistance to rituximab therapy is an important issue.

The mechanisms of action of rituximab are inhibition of proliferation, induction of apoptosis, complement-dependent cytotoxicity, and antibody-dependent cellular cytotoxicity. A few reports indicate that loss of CD20 expression occurs in some patients with non-Hodgkin's lymphoma during rituximab therapy (8–10), but the relationship between development of resistance to rituximab and changes in rituximab action have not yet been clarified. Heterogeneity of intensity of CD20 expression in replicate analysis of the same sample has been commonly observed by flow cytometric analysis (11). One explanation for this might be the development of resistant subsets of lymphoma cells by mutation. Recently, mutations in the epidermal growth factor receptor have been reported to have a relationship with the differing sensitivity to gefitinib therapy seen in samples from Japanese and American patients (12).

Our experience with resistance began with a patient who had a posterior mediastinal lymphoma that became resistant during

Authors' Affiliations: Departments of [1]Medical Oncology and Hematology, and [2]Pathology, Cancer Institute Hospital; [3]Division of Clinical Chemotherapy and [4]Olympus Bio-imaging Laboratory, Cancer Chemotherapy Center, Japanese Foundation for Cancer Research, Tokyo, Japan; and [5]Nutritional Science Laboratory, Morinaga Milk Co., Kanagawa, Japan

Received 5/28/08; revised 11/18/08; accepted 12/17/08; published OnlineFirst 3/10/09.

Grant support: Ministry of Education, Science, and Culture of Japan; grants for Research on Advanced Medical Technology and for International Health Cooperation Research from the Ministry of Health, Welfare, and Labor of Japan; commercial research grants from Bristol-Myers Squibb and Novartis; other commercial research support from Chugai and Novartis; and honoraria from the speakers' bureau of Chugai and Novartis.

The costs of publication of this article were defrayed in part by the payment of page charges. This article must therefore be hereby marked *advertisement* in accordance with 18 U.S.C. Section 1734 solely to indicate this fact.

Note: Y. Terui and K. Hatake designed the research and wrote the article; Y. Terui, Y. Mishima, N. Sugimura, K. Kojima, T. Sakurai, Y. Mishima, R. Kuniyoshi, A. Taniyama, M. Yokoyama, S. Sakajiri, S. Takahashi, and Y. Ito did the research; K. Takeuchi did the pathologic diagnosis; and C. Watanabe analyzed the data.

Requests for reprints: Kiyohiko Hatake, Department of Medical Oncology and Hematology, Cancer Institute Hospital, Japanese Foundation for Cancer Research, 3-10-6 Ariake, Koto-ku, Tokyo, Japan 135-8550. Phone: 81-3-3570-0465; Fax: 81-3-3570-0343; E-mail: khatake@jfcr.or.jp.

doi:10.1158/1078-0432.CCR-08-1403

Translational Relevance

Rituximab is commonly incorporated into CD20-positive B-cell lymphoma therapy to improve response and prognosis. However, with increasing use, resistance to rituximab is a continuing concern. Although some mechanisms have been explained for resistance to rituximab, CD20 C-terminal mutation was found as one of the mechanism for the first time. In this study, two useful applications will be of concern in the field of medicine of malignant lymphoma. First, because the CD20 C-terminal mutation was detected in only patients with disease progression, a more sensitive assay could be developed to detect CD20 mutations at initial diagnosis. This will be able to predict whether the patients with the CD20 mutation may show relapsed/refractory disease. Second, if the patients have lymphoma cells with this kind of the mutation, it will be possible that they may be treated with other strategies such as other anti-CD20 antibodies with or without radioisotopes and anti-CD22 antibodies with or without calicheamycin. For those reasons, this work will be applied to future important practice of the field of malignant lymphoma.

rituximab plus CHOP therapy. Initially, pathologic examination by computed tomography–guided biopsy and immunohistologic testing showed that the lymphoma cells expressed the CD20 antigen. During rituximab plus CHOP therapy, the patient experienced a massive right pleural effusion with lymphoma cells, and these cells showed loss of CD20 expression. In this article, we analyze the relationships between CD20 mutation, CD20 expression, and relapse after rituximab therapy in 50 patients with lymphoma, including the original index case.

Materials and Methods

Collection of clinical samples. This study was approved by the ethics committee of the chamber of physicians at the Japanese Foundation for Cancer Research, Japan. Written informed consent was obtained from all patients to use the resected samples and to do bone marrow aspirates for research purposes. For this study, all 50 patients with malignant lymphoma who underwent lymph node biopsy and bone marrow aspiration at the Cancer Institute Hospital of the Japanese Foundation for Cancer Research between February 1, 2003, and November 30, 2004, were assessed prospectively. After histopathologic examination, the malignancies were classified according to WHO lymphoma criteria. Forty-three patients received R-CHOP (rituximab 375 mg/m^2 weekly for 8 cycles and cyclophosphamide 750 mg/m^2, doxorubicin 50 mg/m^2, vincristine 1.4 mg/m^2, and prednisolone 60 mg/m^2) therapy. Three of them underwent radiotherapy to a total dose of 35 to 45 Gy after R-CHOP, and one of them received radiotherapy before R-CHOP. One patient received a therapy of rituximab 375 mg/m^2 weekly for 8 cycles and cyclophosphamide 750 mg/m^2, vincristine 1.4 mg/m^2, and prednisolone 60 mg/m^2. Five patients received rituximab monotherapy (375 mg/m^2 weekly for 8 cycles). For one patient, rituximab-VP-16 was given as rituximab 375 mg/m^2 weekly for 8 cycles, and etoposide 50 mg was administered orally for 2 of every 4 wks.

Fresh lymphoma cells were collected from 50 patients with non-Hodgkin's lymphoma (diffuse large B cell, n = 22; follicular, n = 7; mucosa associated lymphoid tissue, n = 16; chronic lymphocytic leukemia, n = 2; small lymphocytic lymphoma, n = 1; lymphoplasmacytic, n = 1; mantle cell lymphoma, n = 1). In 9 of the 50 patients, analysis of the *CD20* gene was done after disease progression.

Surface markers. The CD19-positive cells isolated by a magnetic cell sorting system were stained with phycoerythrin-conjugated anti-CD19 (BD Biosciences) and phycoerythrin-conjugated anti-CD20 antibodies. Flow cytometry was done by FACscan (Becton Dickinson). Intensity of CD20 expression was normalized by comparison against a control and expressed as the mean fluorescence intensity ratio. Rituximab was labeled with Alexa Fluor 488 molecule (Invitrogen) in accordance with the manufacturer's instructions.

Assessment of mutations and expression. Genomic DNA and total RNA were extracted from CD19-positive lymphoma cells in TRIzol reagent (Invitrogen) using the supplied protocol. One microgram of RNA was reverse transcribed with Moloney murine leukemia virus reverse transcriptase (BD Biosciences) using oligo(dT)$_{17}$ according to the manufacturer's instruction. Genomic PCR of five of the eight exons of the *CD20* gene was done using BD Advantage 2 polymerase. Reverse transcription-PCR (RT-PCR) was also done using the following pairs of primers containing *Bam*HI and *Sal*I sites to amplify the full-length transcript and selected exon pairs: exons 3 and 4, 5 and 6, and 7 and 8. PCR amplification was carried out with the Hot Start/Amplimax method with the following temperature cycling parameters: 95°C for 30 s, 58°C for 30 s, 68°C for 1 min for 25 cycles, and a final extension at 68°C for 3 mins. The primer pair sequences used for amplification are available as below.

Genomic PCR was done using the following primers with five of eight exons of the CD20 gene, respectively: Forward primer for exon 3, 5′-CCTTTCTCAGAACTCAGC AGTAGGCCTTGC-3′; reverse primer for exon 3, 5′-ACTGACTTACCCCCAAAGTCTTAGATTCCC-3′; forward primer for exon 4, 5′-CTCTCCCCAGGCTGTCCAGATTATGAATGG-3′; reverse primer for exon 4, 5′-TTTTACTCACCATAATGCCTCCCCAGAGAG-3′; forward primer for exon 5, 5′-CTCCTCTATCTCCTGTCTTGCCCACCCCCT-3′; reverse primer for exon 5, 5′-AAAAAATAGGTACTTCTCTGACATGTGGGA-3′; forward primer for exon 6, 5′-CATTTCAGGTCAAAGGAAAAATGAT-3′; reverse primer for exon 6, 5′-ACTTACCAAGAACACTTACCAAGAA-3′; forward primer for exon 7, 5′-TGTTTTTCAGGGCATTTTGTCAGTGATGCT-3′; reverse primer for exon 7, 5′-ACTACTACTTACAGATTTGGGTCTGGAGCA-3′; forward primer for exon 8, 5′-TTTCTGTTTTAGAACATAGTTCTCCTGTCA-3′; and reverse primer for exon 8, 5′-CAGAAAACAGAAGAAATCACTTAAGGAGAG-3′.

Table 1. Patient characteristics

Histology	Treatment	*n*	Analysis of PD sample
MALT	R-CHOP	11	1
	R	3	1
	R-VP16	1	
	R-CHOP → RTx	1	
FL	R-CHOP	5	2
	R	1	
	R-CHOP → RTx	1	
DLBCL	R-CHOP	21	2
	RTx → R-CHOP	1	1
CLL/SLL	R-CHOP	2	1
	R	1	
Lymphoplasmacytic	R-COP	1	
MCL	CHOP+ RTx →R	1	1

Abbreviations: CLL/SLL, chronic lymphocytic leukemia or small lymphocytic lymphoma; COP, cyclophosphamide, vincristine, and prednisone; DLBCL, diffuse large B-cell lymphoma; FL, follicular lymphoma; MALT, mucosa-associated lymphoid tissue; MCL, mantle cell lymphoma; PD, progressive disease; R, rituximab; RTx, radiation therapy; VP16, etoposide.

RT-PCR was also done using the following pairs of primers with *Bam*HI and *Sal*I sites for full length and three parts of exons (exons 3 and 4, 5 and 6, and 7 and 8), respectively: Forward primer for full length, 5′-CGCGGATCCGCGATGACAACACCCAGA-3′; reverse primer for full length, 5′-TCCCCCGGGGGATTAAGGAGAGCTGTC-3′; forward primer for exons 3 and 4, 5′-ATGACAACACC CAGAAATTCAGTAAATGGG-3′; reverse primer for exons 3 and 4, 5′-CATAATGCCTCCCCAGAGAGGG-TACCACAC-3′; forward primer for exons 5 and 6, 5′-TATATTATTTCCG-GATCACTCCTGGCAGCA-3′; reverse primer for exons 5 and 6, 5′-CCAAGAACAGAGATTGTATGCTGTAACAGT-3′; forward primer for exons 7 and 8, 3′-GCATTTTGTCAGTGATGCTGATCTTTGCCT-5′; and reverse primer for exons 7 and 8, 5′-TTAAGGAGAGCT GTCATTTTC-TATTGGTG A-3′. The following pair of primers for glyceraldehyde-3-phosphate dehydrogenase was used as a housekeeping gene control: forward primer, 5′-CCTTCATTGACCTCAACTAC-3′, and reverse primer, 5′-AGTGATGGCATGGACTGTGGT-3′.

Direct sequence analysis of genomic DNA and PCR product was done by ABI PRISM 3100 (Invitrogen) as described in previous reports (13, 14).

Cloning and expression of CD20 mutations. The PCR product was subcloned into mammalian expression vector pTARGET (Promega) using a single 3-T overhang into the cloning site. pTARGET vectors with CD20 mutants were stably introduced into the chronic myelogenous leukemia cell line K562 by electroporation and selected with G418 (Invitrogen).

In vitro *translation assay.* The *CD20* mutant genes in the pTARGET vector were transcribed and translated using an *in vitro* translation kit (Promega) according to the protocol. In brief, 1 μg of DNA was added to the *in vitro* translation reaction mixture. After adding 1 μCi of ^{35}S-methionine, the reaction mixture was incubated at 30°C for 1 h. After electrophoresis of the labeled products, the gel was dried and autoradiography was done.

In vivo *transfection assay.* Wild-type and mutant sequences were stably transfected into K562 cells (K562/mock, K562/WT, K562/CD-1, K562/CD-2, and K562/CD-3); after which, flow cytometric analysis was done and confocal laser scanning microscopy was used for imaging analysis (FV1000, Olympus). Immunohistochemistry was done on mock, wild-type, CD-1, CD-2, and CD-3 mutant-transfected K562 cells using a biotin-free dextran polymer system (Envision+, DAKO).

Antibody against CD20 N-terminal peptide. The peptide corresponding to amino acids 23 to 36 of CD20, MQSGPKPLFRRMSS, was synthesized, and a polyclonal antibody against the peptide was raised in the rabbit by Scrum, Inc. The antiserum was purified using an Immunopure IgG purification kit (Pierce Biotechnology, Inc.) according to the manufacturer's protocol. For Western blot analysis with this antibody, the cells were then washed once with PBS and lysed with 1× sample buffer. After electrophoresis on 10% to 20% gradient gels (Daiichikagaku), Western blot analysis was done with primary polyclonal anti-CD20 N-terminus antibody (dilution, 1:1,000) and secondary horse radish peroxidase-conjugated anti-rabbit immunoglobulin antibody (Santa Cruz Biotechnology, Inc.). Detection was done using an enhanced chemiluminescence system (GE Healthcare UK Ltd.).

Immunohistochemistry. Sections (4-μm thick) were cut and mounted on poly-L-lysine-coated slides. Immunohistochemistry was done using a biotin-free dextran polymer system (Envision+, DAKO). Briefly, after deparaffinization in xylene and rehydration using ethanol/water dilutions, antigen retrieval was done by placing the sections in preheated 0.01 mol/L citrate buffer (pH 6) for 40 mins at 97°C, followed by 20 mins at room temperature. Endogenous peroxidase was blocked by immersion in 3% hydrogen peroxide for 5 mins at room temperature. The sections were incubated with the anti-N-terminus of CD20 rabbit polyclonal antibody (1:400) for 30 mins at room temperature. The antibody was detected with Envision+, and the reactions were visualized by incubating the sections with diaminobenzidene (DAB+, DAKO). The sections were counterstained with hematoxylin; all staining procedures were done in a DAKO Autostainer.

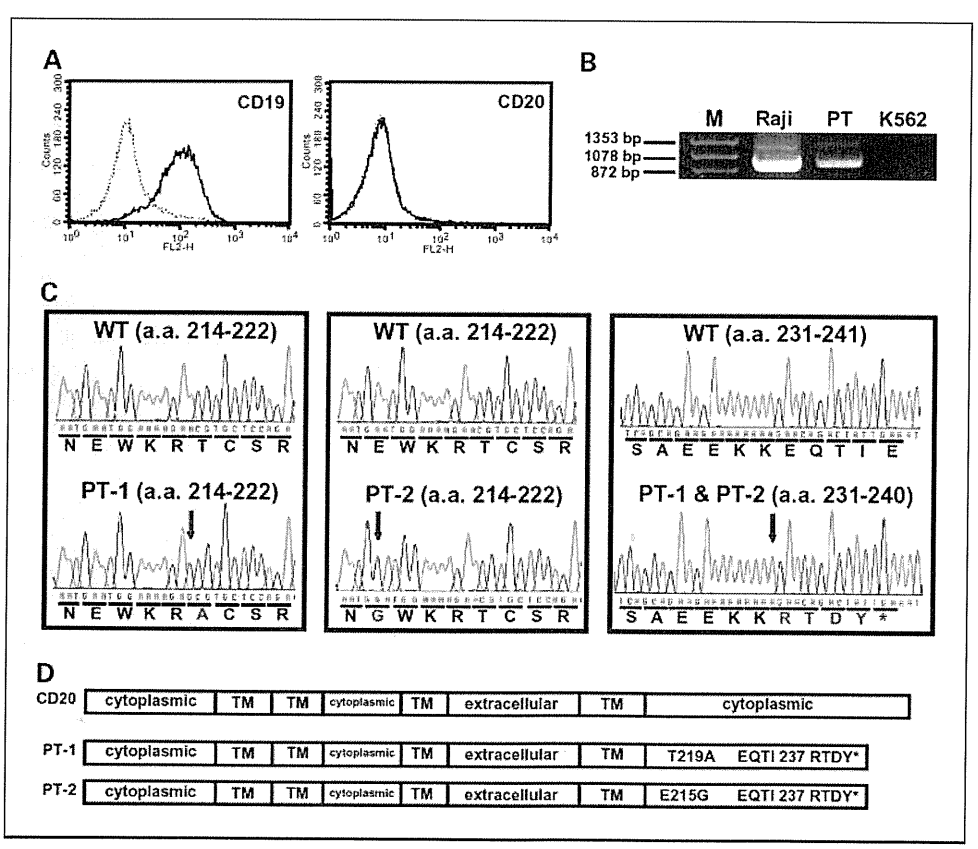

Fig. 1. CD20 expression and mutation analysis in CD19-positive lymphoma cells from a patient with posterior mediastinal lymphoma. *A,* flow cytometry for CD19 and CD20 cells. *B,* RNA analysis. RT-PCR using CD20 primers. Total RNAs from Raji and K562 cells were used as positive and negative controls, respectively. *C,* nucleic acid sequence analysis. Arrows, replacement or insertion of a nucleic acid. Top and bottom, sequences of nucleic acids and amino acids of wild-type and mutant (PT-1 and PT-2) sequences corresponding to amino acids 214 to 240 and 231 to 241. WT, wild type; a.a., amino acids. *D,* amino acid sequence analysis. Two clones (PT-1 and PT-2) showed replacement of one amino acid and a partial deletion in the C-terminal cytoplasmic domain. Four amino acids (E237-I240) were also changed at the C-terminus (R237-Y240). PT, patient.

Table 2. Mutations found in 11 patients

Groups	Mutated domains	Amino acid sequence from mutation	Classification	Therapy	Biopsy after PD
Group 1					
C-terminal deletion (truncation) CD-1	C-terminal cytoplasmic	I211S	FL	R-CHOP	Yes
CD-2	C-terminal cytoplasmic	EQT123 RTDY	DLBCL	R-CHOP	No
CD-3*	C-terminal cytoplasmic	T219A: EQT123RTDY	DLBCL*	RTx → R-CHOP	Yes*
CD-4*	C-terminal cytoplasmic	E215G: EQT123RTDY	DLBCL*	RTx → R-CHOP	Yes*
CD-5	Second transmembrane fused to C-terminal cytoplasmic	SLLAATEKNSRKCLVKGKMIMNSLSLFAAIS-GMILSIMDIL fused to ITPGSNGEKLQEV-FGQRKNDNEFIEPLCCHFWNDSFNHGHT	MCL	CHOP + RTx → R	Yes
Group 2					
Extracellular	Extracellular	T180A	DLBCL	R-CHOP	No
Group 3					
Transmembrane	Third transmembrane	F125L	CLL/SLL	R	No
Group 4					
Early termination	N-terminal cytoplasmic	MYIHVLKLSHHFMSTVH	MALT	R-CHOP	No
	N-terminal cytoplasmic	MGLSRQSQ	DLBCL	R-CHOP	No
	N-terminal cytoplasmic	MGLSRQSQ	DLBCL	R-CHOP	No
	N-terminal cytoplasmic	MTHPEIQ	MALT	R-CHOP	No
	N-terminal cytoplasmic	MTHPEIQ	DLBCL	R-CHOP	No

*Clones CD-3 and CD-4 are from the same patient.

Clinical parameters. Time to progression was calculated from the date of initiation of rituximab therapy to the date of detection of progressive disease or to the date of last contact.

Statistical analysis. Statistical analysis was done using StatView version 5.0 and InStat version 2.00 software (SAS Institute, Inc.). Statistical comparisons were done by Kruskal-Wallis nonparametric ANOVA test and confirmed by Student's t test, with $P < 0.05$ interpreted as a significant difference. Time to progression was analyzed by the Kaplan-Meier method using Dr. SPSS II software (SPSS Japan, Inc.), and the log-rank test was used for univariate analysis.

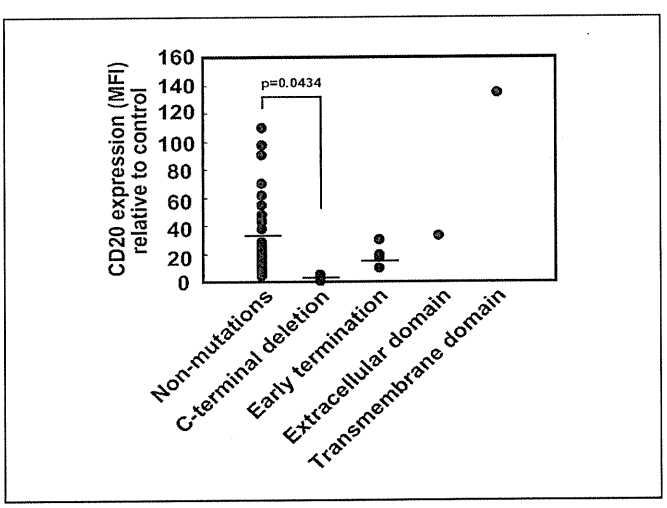

Fig. 2. Relationship between mutations and CD20 expression. Mean fluorescence intensity of CD20 relative to the control was assessed in CD19-positive cells from clinical samples by flow cytometric analysis. Fifty cases were classified as nonmutations or as mutations and grouped according to the domain affected (C-terminal deletion, extracellular domain, early termination, and transmembrane domain). MFI, mean fluorescence intensity.

Results

CD20 mutations. Patient characteristics and timing of mutation analysis are shown in Table 1. The index case of a female with posterior mediastinal lymphoma developing resistance during rituximab plus CHOP therapy was included in this nucleic acid analysis. Although these lymphoma cells were CD19 positive and CD20 negative on flow cytometric analysis (Fig. 1A), CD20 mRNA was detectable by RT-PCR (Fig. 1B). In our study, genomic PCR and RT-PCR were done with the primers for five of the eight exons in the *CD20* genes. In exon 8, sequence analysis for genomic DNA and the PCR product revealed that there were some clones with frameshifts due to insertion of one adenine residue. To confirm this result, the PCR products were subcloned into mammalian expression vector pTARGET, and analysis on the ABI sequencer detected the same frameshift mutation in combination with two different point mutations (Fig. 1C). Four of the 10 clones identified showed the same frameshift mutation in genomic DNA that had been detected by PCR. Of the two point mutations, both resulted in replacement of one amino acid (T219A and E215G) and both were seen in combination with a partial deletion frameshift mutation in the C-terminal cytoplasmic domain (changing the C-terminal four amino acids from EQTI to RTDY; Fig. 1D).

RNA samples from 49 other patients with non-Hodgkin's lymphoma were investigated retrospectively by RT-PCR analysis.

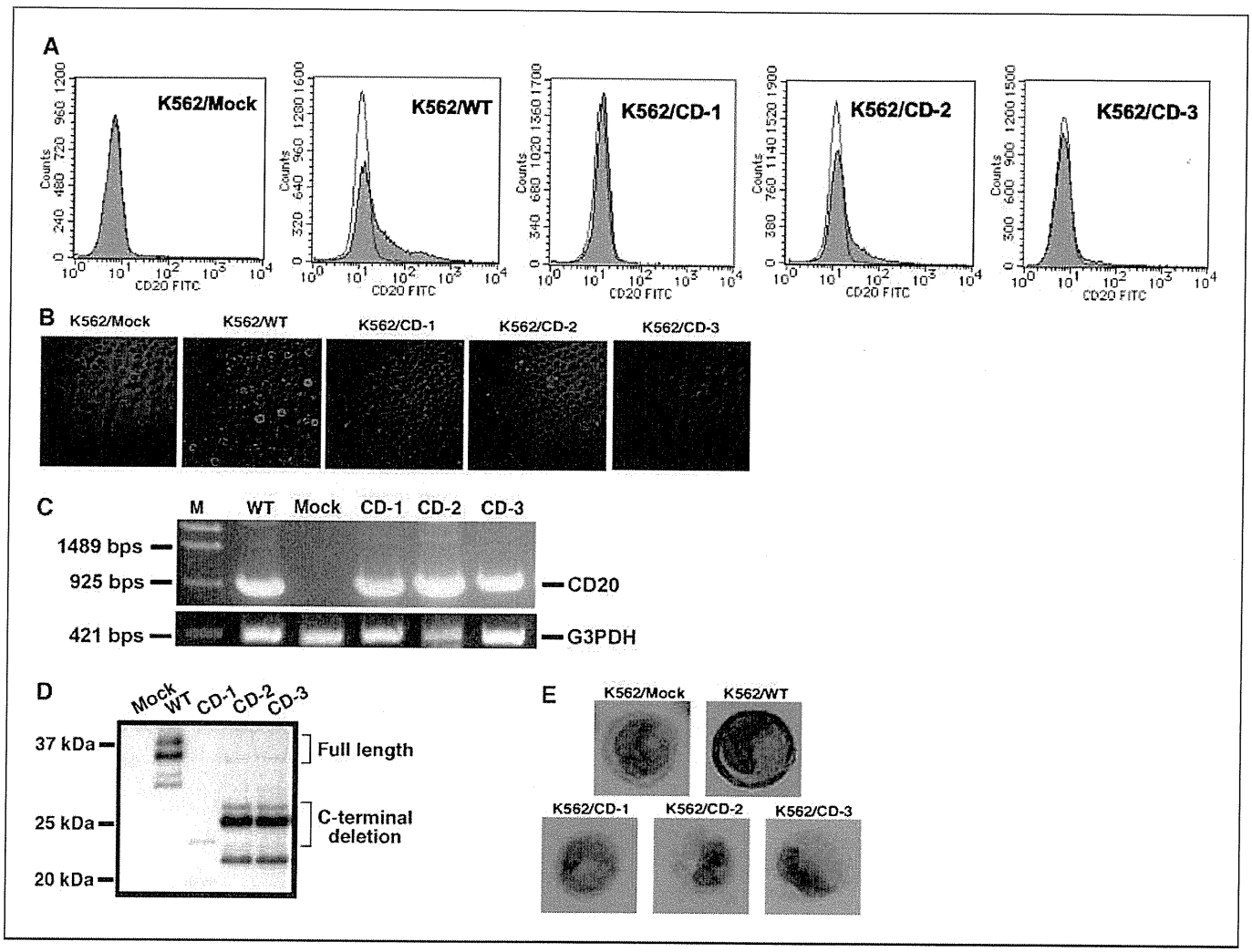

Fig. 3. CD20 expression in mutants CD-1, CD-2, and CD-3. Wild-type and mutant sequences were stably transfected into K562 cells (K562/mock, K562/WT, K562/CD-1, K562/CD-2, and K562/CD-3); after which, flow cytometric analysis was done with Alexa Fluor 488–labeled rituximab, and confocal laser scanning microscopy with Alexa Fluor 488–labeled rituximab was used for imaging analysis (FV1000, Olympus). *A*, flow cytometry results. *B*, confocal laser scanning microscopy results. *C*, RT-PCR results using total RNA. The PCR product of glyceraldehyde-3-phosphate dehydrogenase was loaded as a housekeeping gene control. *D*, Western blotting results using anti–CD20 N-terminus antibody. *E*, immunohistochemistry results. Cells were stained for CD20 expression with anti–CD20 N-terminus antibody.

All patients had received rituximab with or without other chemotherapy or radiotherapy, and in 9 of the 50 patients, fresh samples for the analysis were taken after disease progression (Table 1). We found heterogeneity at the nucleic acid level, with several different CD20 mutation types identified by DNA analysis, which could be grouped according to their location (Table 2). The C-terminal cytoplasmic domain was affected in patients classified in Group 1. Table 2 presents the group 1 mutations seen in the index case (CD-3, CD-4), in which the adenine insertion frameshift was observed without detection of the additional point mutation (CD-2) and a partial deletion stopped at amino acid S211 (CD-1). Finally, a replacement of ITPGSNGEKLQEVFGQRKNDNEFIEPLCC-HFWNDSFNHGHT at S162 in the second transmembrane domain caused the C-terminal cytoplasmic domain to be defective (CD-5). The samples from three of the four patients in group 1 were taken after disease progression.

In group 2, the extracellular domain was altered by replacement of an amino acid (T180A). In group 3, replacement of an amino acid (F125L) altered the third transmembrane domain. The four patients in group 4 had a stop codon detected close to the 5 site of the *CD20* gene, which may produce a short peptide. In these cases, a second methionine following the stop codon may initiate transcription of a long peptide.

Relationship between CD20 expression and CD20 mutations. The relationship between groups of mutations and CD20 expression were examined in fresh CD19-positive cells from patients with non-Hodgkin's lymphoma. To observe which group of CD20 mutations was related to down-regulation of CD20 expression, the mean fluorescence intensity of CD20 expression relative to the control was examined in each group (Fig. 2). There was a significant difference in CD20 expression between wild-type and C-terminal deletion mutation groups (mean difference, 24.0; $P < 0.01$), but this was not the case for wild type compared with early termination groups (mean difference, 3.1; $P > 0.05$) or between C-terminal deletions mutation and early termination groups (mean difference, -21.0; $P > 0.05$). The CD20 expression seen in group 1 [mean fluorescence intensity, 3.26; 95% confidence interval (95% CI), 0.09-6.89] significantly decreased compared with wild type

(mean fluorescence intensity, 30.8; 95% CI, 22.4-39.2; $P < 0.05$; two-sided Student's t test), whereas that of the early termination group (mean fluorescence intensity, 19.5; 95% CI, 10.7-28.4) was not significantly different from wild type. In addition, there was no significant difference in the mean fluorescence intensity among between the different subtypes of B-cell lymphomas such as diffuse large B-cell lymphoma (mean fluorescence intensity, 35.9; 95% CI, 23.5-48.3), mucosa-associated lymphoid tissue (mean fluorescence intensity, 32.8; 95% CI, 18.3-47.3), follicular lymphoma (mean fluorescence intensity, 17.9; 95% CI, 11.7-24.1), and chronic lymphocytic leukemia or small lymphocytic lymphoma (mean fluorescence intensity, 51.82; 95% CI, 1-133.3), and the specimens collected upon progression of disease (mean fluorescence intensity, 18.5; 95% CI, 7.3-29.7) did not significantly show low expression of CD20 as compared with those at diagnosis (mean fluorescence intensity, 36.4; 95% CI, 25.7-47.1). These results suggest that the C-terminal deletion mutation is strongly associated with decreased or absent CD20 expression. One of the reported mechanisms of action for rituximab is complement-dependent cytotoxicity, which is regulated by some inhibitory factors such as CD46, CD59, and CD55 (15, 16). Because CD55 is a potent inhibitor of rituximab-induced complement-dependent cytotoxicity in bulky lymphomas (17), CD55 expression was examined in the fresh CD19-positive cells from the patients, but no significant difference was detected for CD55 expression on the lymphoma cells (data not shown).

***CD20 production* in vitro *and* in vivo.** The *in vitro* translation and *in vivo* transfection experiments done to examine CD20 production showed that cells with C-terminal deletion mutations (CD-2, CD-3, and CD-4) had lower levels of RNA and protein than cells that were wild type or contained other point mutations (data not shown). To confirm whether C-terminal deletion mutations reduce or eliminate CD20 expression on the cell surface, the mutated genes subcloned into pTARGET were stably transfected into K562 cells (Fig. 3). K562/mock cells and K562 cells did not express CD20 molecules on flow cytometric (Fig. 3A) and microscopic (Fig. 3B) analyses. CD20 expression on K562/CD-1, K562/CD-2, and K562/CD-3 cells was not detected or showed a very low signal on flow cytometric (Fig. 3A) and microscopic (Fig. 3B) analyses. These results were not due to a loss or decrease in CD20 RNA as examined by RT-PCR (Fig. 3C). Mutant products CD-2 and CD-3 were expressed in addition to wild type, although fewer larger size fragments were deleted than that of wild type (Fig. 3D). On immunostaining with anti-N-terminal CD20 antibody, wild-type product was strongly detected on the cell membrane (Fig. 3E); C-terminal deletion mutants were weakly detected in the cytoplasm but not on the cell surface.

Discussion

The results from the original index case suggested that replacement of one amino acid and/or the partial deletion of the C-terminus might cause loss of CD20 expression, and hence, analysis was expanded retrospectively to include 50 patients. In these 50 patients, the overall response rate was 92% (46 of 50) after rituximab therapy, but two of these patients developed progressive disease after achieving a partial response. In fact, two of the three patients with mutations detected after disease progression (Table 2) showed C-terminal deletions. Because C-terminal deletion mutations are associated with reduced or absent expression of CD20, we investigated whether there was any significant difference in response and prognosis for patients after rituximab therapy between this group and the wild-type group. Complete response rates with rituximab therapy were 49% in the wild-type group but only 25% in the C-terminal deletion mutation group. No statistically significant difference between these groups was found because of the low number of cases in the C-terminal deletion mutation group. After rituximab therapy, median time to progression was 31 months (95% CI, 18-44 months), 30 months (95% CI, 31-37 months), and 7 months (95% CI, 0-18 months) for the wild-type, early-termination, and C-terminal deletion groups, respectively.

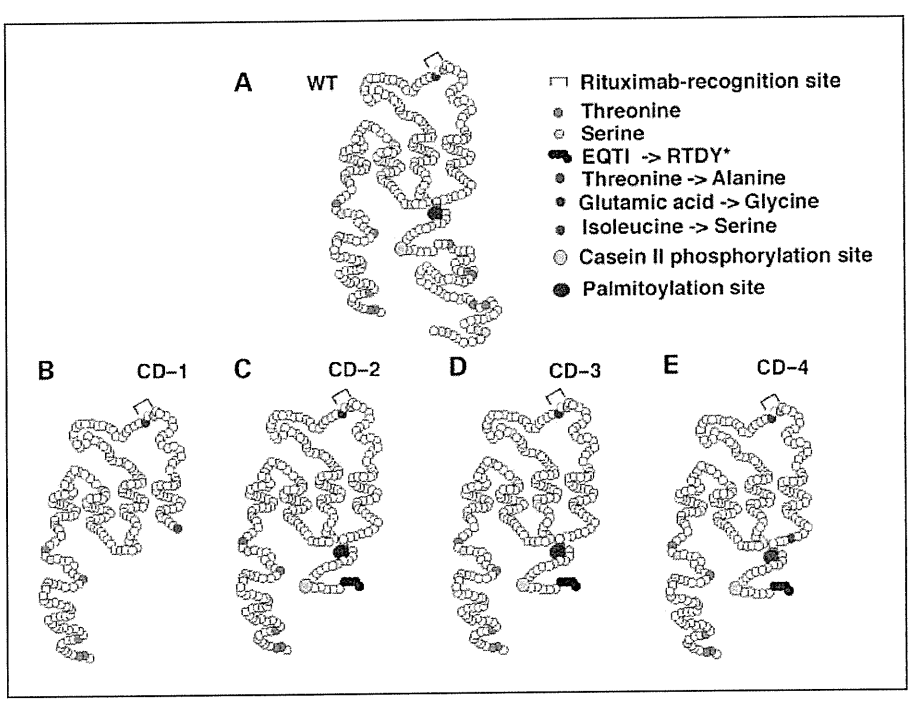

Fig. 4. The structures of wild-type and mutant CD20. Wild-type CD20 is composed of 297 amino acids (*A*), and casein kinase 2 and calcium/calmodulin-dependent protein kinase 2 phosphorylation sites are expected in its C-terminal cytoplasmic domain. C-terminal deletion mutants are shown as CD-1 (*B*), CD-2 (*C*), CD-3 (*D*), and CD-4 (*E*).

Although the tumor types and the treatment received were heterogeneous and only four patients had C-terminus mutations, the C-terminal deletion mutation seems to be associated with short time to progression and early relapse of disease.

The mean fluorescence intensity results indicate that the C-terminal deletion mutation is strongly associated with decline or disappearance of CD20 expression, and the results of expression studies suggest that C-terminal deletions may mask CD20 expression on the cell surface or affect duration of cell surface exposure to CD20.

Heterogeneity of intensity of CD20 expression in replicate analysis of the same sample is commonly observed with flow cytometric analysis (11). This indicates that subclones expressing lower CD20 levels are present in CD20-positive lymphoma cells and that surviving clones may cause resistance or relapse after rituximab therapy. It is thus vital that these clones are killed to protect patients from the risk of resistance or relapse. Jazirehi et al. (18) have reported that rituximab-resistant lymphoma cells can be chemosensitized following treatment with pharmacologic inhibitors such as bortezomib that target survival/antiapoptotic pathways. Structurally, the C-terminal cytoplasmic domain of CD20 possesses some phosphorylation sites for protein kinases such as casein kinase 2 and calcium/calmodulin-dependent protein kinase 2 (Fig. 4A). S239 is predicted to be phosphorylated by casein kinase 2, and S221 and S225 are potential calcium/calmodulin-dependent protein kinase 2 phosphorylation sites (19, 20); however, the significance of the phosphorylation of these sites remains to be clarified. On the other hand, the cytoplasmic region of CD20 (amino acids 219-225) is known to be required for its redistribution to the detergent-insoluble membrane compartment, which plays an important role in the action of rituximab (21). One of four C-terminal deletion mutants (Fig. 4B) reported here had lost several predicted phosphorylation sites such as casein kinase 2 and calcium/calmodulin-dependent protein kinase 2 in contrast to the other three mutants (Fig. 4C-E). Another feature of the distal region in the C-terminus is the presence of a glutamic acid–rich region (19, 22). The sequence of E233 to E292 is predicted to be a glutamic acid–rich region profile using the Motif Scan program and PROSITE database, and this region may play an important role in retention of calcium ions, analogous to the role of bone sialoprotein (23). It has been reported that B lymphocytes are activated and CD20 is up-regulated by phorbol myristate acetate and ionomycin (24), suggesting that intracellular calcium ions participate in CD20 expression. However, we have shown that the C-terminal deletion mutant CD20 was produced as RNA in the cells but was not detected as a protein on the cell surface. This may be a consequence of the rapid turnover of CD20 mutant molecules between the cell surface and cytoplasm, resulting in exposure at the cell surface that is too brief for detection by immunofluorescence. If so, anti-CD20 antibody linked to anticancer drugs such as ozogamicin could be a useful treatment approach for patients with this mutation.

Two classes of mutations are spontaneous mutations and induced mutations caused by mutagens (25, 26). Spontaneous mutations on the molecular level include tautomerism, depurination, deamination, transition, and transversion, whereas chemicals such as alkylating agents and radiation can cause induced mutations on the molecular level. Alkylating agents such as cyclophosphamide in CHOP therapy can mutate replicating and nonreplicating DNA and has certain effects that then lead to transitions, transversions, or deletions. In this study, 44 patients had received CHOP therapy with rituximab, and three of them (6.9%) had C-terminal deletion mutants when they showed progression disease after R-CHOP therapy. One patient showed C-terminal deletion before R-CHOP therapy. Because Ragg et al. (27) has reported that overexpression and mutant of methylguanine methyltransferase protects mice against effect of alkylators, loss of function of this enzyme may induce gene mutagenesis by alkylating reagents such as cyclophosphamide. Moreover, 4 of 50 cases received radiation therapy during the treatment, and radiation therapy before administration of rituximab was given to two cases, which showed C-terminal deletion mutation after progression disease. Radiation before rituximab administration may also be related to mutagenesis of CD20 gene. Because one patient showed C-terminal deletion mutation before immunochemotherapy, we also need to consider clonal selection of CD20 after R-CHOP therapy. Moreover, microsatellite instability is known to be one of the mechanisms of gene mutation (28). Although microsatellite instability was examined as the cause of CD20 mutation in four patients with the C-terminal deletion mutation, it was not observed in their lymphoma cells (data not shown). Because two of these patients had received radiotherapy before rituximab therapy, radiation may have caused the CD20 mutation before treatment. However, some researchers have found that rituximab-resistant cells with low CD20 levels of rituximab have the same *CD20* gene sequence as that of sensitive cells (29, 30), suggesting that various or other mechanisms may contribute to CD20 down-regulation.

Although we found the C-terminal deletion mutation clones more often in patients with disease progression than at initial diagnosis, C-terminal deletion mutation was also strongly related to a shortening of the drug-free duration. Clinical prognostic factors for B-cell malignant lymphoma are well described and include age, Ann Arbor clinical stage, hemoglobin level, number of affected lymph nodes, and lactate dehydrogenase level (31, 32). Moreover, DNA microarray analysis implicates expression of several genes, including *BCL2*, *BCL6*, and *ZAP70*, as denoting poor prognosis in B-cell malignant lymphoma (33–36). However, there has been no report about gene mutations within molecular markers of lymphoma, such as the *CD20* gene. Here, we have presented the first data showing that a *CD20* gene mutation is related to a decline in CD20 expression and poor patient outcome. Because the mutation was detected in patients with disease progression, a more sensitive assay should be developed to detect CD20 mutations at initial diagnosis.

In conclusion, we found that C-terminal deletion mutations of CD20 were related to relapse/resistance after rituximab therapy, and screening for these mutations should be done in patients with disease progression after partial remission.

Disclosure of Potential Conflicts of Interest

The authors have received a commercial research grant from Chugai and honoraria from the speakers' bureau of Chugai.

Acknowledgments

We thank Dr. Dovie Wylie for the English editing and correction; Tomomi Sagawa, Sayuri Minowa, Noriko Yamamichi, and Harumi Shibata for the technical assistance; and Ayako Sakai for the illustration description.

References

1. Arin MJ, Hunzelmann N. Anti-B-cell-directed immunotherapy (rituximab) in the treatment of refractory pemphigus—an update. Eur J Dermatol 2005;15: 224–30.
2. Emens LA. Trastuzumab: targeted therapy for the management of HER-2/neu-overexpressing metastatic breast cancer. Am J Ther 2005;12:243–53.
3. Ferrara N, Hillan KJ, Novotny W. Bevacizumab (Avastin), a humanized anti-VEGF monoclonal antibody for cancer therapy. Biochem Biophys Res Commun 2005;333:328–35.
4. Vasir JK, Labhasetwar V. Targeted drug delivery in cancer therapy. Technol Cancer Res Treat 2005;4: 363–74.
5. Coiffier B. State-of-the-art therapeutics: diffuse large B-cell lymphoma. J Clin Oncol 2005;23:6387–93.
6. Schmits R, Schmitz N, Pfreundschuh M. The best treatment for diffuse large B-cell lymphoma: a German perspective. Oncology (Huntingt) 2005;19:16–25.
7. Hagenbeek A, Lewington V. Report of a European consensus workshop to develop recommendations for the optimal use of (90)Y-ibritumomab tiuxetan (Zevalin) in lymphoma. Ann Oncol 2005;16:786–92.
8. Haidar JH, Shamseddine A, Salem Z, et al. Loss of CD20 expression in relapsed lymphomas after rituximab therapy. Eur J Haematol 2003;70:330–2.
9. Alvaro-Naranjo T, Jaen-Martinez J, Guma-Padro J, Bosch-Princep R, Salvado-Usach MT. CD20-negative DLBCL transformation after rituximab treatment in follicular lymphoma: a new case report and review of the literature. Ann Hematol 2003;82:585–8.
10. Rawal YB, Nuovo GJ, Frambach GE, Porcu P, Baiocchi RA, Magro CM. The absence of CD20 messenger RNA in recurrent cutaneous B-cell lymphoma following rituximab therapy. J Cutan Pathol 2005;32: 616–21.
11. Smith MR. Rituximab (monoclonal anti-CD20 antibody): mechanisms of action and resistance. Oncogene 2003;22:7359–68.
12. Paez JG, Janne PA, Lee JC, et al. EGFR mutations in lung cancer: correlation with clinical response to gefitinib therapy. Science 2004;304:1497–500.
13. Metaxa-Mariatou V, Papadopoulos S, Papadopoulou E, et al. Molecular analysis of GISTs: evaluation of sequencing and dHPLC. DNA Cell Biol 2004;23: 777–82.
14. Willmore C, Holden JA, Zhou L, Tripp S, Wittwer CT, Layfield LJ. Detection of c-kit-activating mutations in gastrointestinal stromal tumors by high-resolution amplicon melting analysis. Am J Clin Pathol 2004; 122:206–16.
15. Bellosillo B, Villamor N, Lopez-Guillermo A, et al. Complement-mediated cell death induced by rituximab in B-cell lymphoproliferative disorders is mediated *in vitro* by a caspase-independent mechanism involving the generation of reactive oxygen species. Blood 2001;98:2771–7.
16. Takei K, Yamazaki T, Sawada U, Ishizuka H, Aizawa S. Analysis of changes in CD20, CD55, and CD59 expression on established rituximab-resistant B-lymphoma cell lines. Leuk Res 2006;30:635–1.
17. Terui Y, Sakurai T, Mishima Y, et al. Blockade of bulky lymphoma-associated CD55 expression by RNA interference overcomes resistance to complement-dependent cytotoxicity with rituximab. Cancer Sci 2006;97:72–9.
18. Jazirehi AR, Vega MI, Bonavida B. Development of rituximab-resistant lymphoma clones with altered cell signaling and cross-resistance to chemotherapy. Cancer Res 2007;67:1270–81.
19. Cragg MS, Walshe CA, Ivanov AO, Glennie MJ. The biology of CD20 and its potential as a target for mAb therapy. Curr Dir Autoimmun 2005;8:140–74.
20. Riley JK, Sliwkowski MX. *CD20*: a gene in search of a function. Semin Oncol 2000;27:17–24.
21. Polyak MJ, Tailor SH, Deans JP. Identification of a cytoplasmic region of CD20 required for its redistribution to a detergent-insoluble membrane compartment. J Immunol 1998;161:3242–8.
22. Hunter GK, Goldberg HA. Modulation of crystal formation by bone phosphoproteins: role of glutamic acid-rich sequences in the nucleation of hydroxyapatite by bone sialoprotein. Biochem J 1994;302: 175–9.
23. Shankar G, GadekTR, Burdick DJ, Davison I, Mason WT, Horton MA. Structural determinants of calcium signaling by RGD peptides in rat osteoclasts: integrin-dependent and -independent actions. Exp Cell Res 1995;219:364–71.
24. DeBenedette M, Snow EC. Induction and regulation of casein kinase II during B lymphocyte activation. J Immunol 1991;147:2839–45.
25. Odegard VH, Schatz DG. Targeting of somatic hypermutation. Nat Rev Immunol 2006;6:573–83.
26. Lalonde R, Strazielle C. Spontaneous and induced mouse mutations with cerebellar dysfunctions: behavior and neurochemistry. Brain Res 2007;1140: 51–74.
27. Ragg S, Xu-Welliver M, Bailey J, et al. Direct reversal of DNA damage by mutant methyltransferase protein protects mice against dose-intensified chemotherapy and leads to *in vivo* selection of hematopoietic stem cells. Cancer Res 2000;60:5187–95.
28. Inoue K, Kohno T, Takakura S, Hayashi Y, Mizoguchi H, Yokota J. Frequent microsatellite instability and BAX mutations in T cell acute lymphoblastic leukemia cell lines. Leuk Res 2000;24:255–62.
29. Tomita A, Hiraga J, Kiyoi H, et al. Epigenetic regulation of CD20 protein expression in a novel B-cell lymphoma cell line, RRBL1, established from a patient treated repeatedly with rituximab-containing chemotherapy. Int J Hematol 2007;86:49–57.
30. Czuczman MS, Olejniczak S, Gowda A, et al. Acquirement of rituximab resistance in lymphoma cell lines is associated with both global *CD20* gene and protein down-regulation regulated at the pretranscriptional and posttranscriptional levels. Clin Cancer Res 2008;14:1561–70.
31. Olejniczak SH, Hernandez-Ilizaliturri FJ, Clements JL, Czuczman MS. Acquired resistance to rituximab is associated with chemotherapy resistance resulting from decreased Bax and Bak expression. Clin Cancer Res 2008;14:1550–60.
32. Solal-Celigny P, Roy P, Colombat P, et al. Follicular lymphoma international prognostic index. Blood 2004;104:1258–65.
33. Sweetenham JW. Diffuse large B-cell lymphoma: risk stratification and management of relapsed disease. Hematology Am Soc Hematol Educ Program. 2005:252–9.
34. Lossos IS, Morgensztern D. Non-Hodgkin's lymphoma in the microarray era. Clin Lymphoma 2004;5: 128–9.
35. Rossi D, Gaidano G. Molecular heterogeneity of diffuse large B-cell lymphoma: implications for disease management and prognosis. Hematology 2002;7: 239–52.
36. Ruiz-Vela A, Piqueras R, Carvalho-Pinto C, et al. ZAP-70 upregulation in transformed B cells after early pre-BI cell transplant into NOD/SCID mice. Oncogene 2005;24:5119–24.

Cell Transplantation, Vol. 18, pp. 381–389, 2009

0963-6897/09 $90.00 + .00
E-ISSN 1555-3892
www.cognizantcommunication.com

ERas Is Expressed in Primate Embryonic Stem Cells But Not Related to Tumorigenesis

Yujiro Tanaka,*¶[1] Tamako Ikeda,*[1] Yukiko Kishi,* Shigeo Masuda,* Hiroaki Shibata,*‡ Kengo Takeuchi,§ Makoto Komura,¶ Tadashi Iwanaka,¶ Shin-ichi Muramatsu,† Yasushi Kondo,# Kazutoshi Takahashi,** Shinya Yamanaka,** and Yutaka Hanazono*

*Division of Regenerative Medicine, Center for Molecular Medicine, Jichi Medical University, Tochigi, Japan
†Division of Neurology, Department of Internal Medicine, Jichi Medical University, Tochigi, Japan
‡Tsukuba Primate Research Center, National Institute of Biomedical Innovation, Ibaraki, Japan
§Department of Pathology, Cancer Institute Hospital, Tokyo, Japan
¶Department of Pediatric Surgery, Graduate School of Medicine, University of Tokyo, Tokyo, Japan
#Mitsubishi Tanabe Pharma, Osaka, Japan
**Center for iPS Cell Research and Application, Institute for Integrated Cell-Material Sciences, Kyoto University, Kyoto, Japan

The ERas gene promotes the proliferation of and formation of teratomas by mouse embryonic stem (ES) cells. However, its human orthologue is not expressed in human ES cells. This implies that the behavior of transplanted mouse ES cells would not accurately reflect the behavior of transplanted human ES cells and that the use of nonhuman primate models might be more appropriate to demonstrate the safety of human ES cell-based therapies. However, the expression of the ERas gene has not been examined in nonhuman primate ES cells. In this study, we cloned the cynomolgus homologue and showed that the ERas gene is expressed in cynomolgus ES cells. Notably, it is also expressed in cynomolgus ES cell-derived differentiated progeny as well as cynomolgus adult tissues. The ERas protein is detectable in various cynomolgus tissues as assessed by immunohistochemisty. Cynomolgus ES cell-derived teratoma cells, which also expressed the ERas gene at higher levels than the undifferentiated cynomolgus ES cells, did not develop tumors in NOD/Shi-*scid*, IL-2Rγ^{null} (NOG) mice. Even when the ERas gene was overexpressed in cynomolgus stromal cells, only the plating efficiency was improved and the proliferation was not promoted. Thus, it is unlikely that ERas contributes to the tumorigenicity of cynomolgus cells. Therefore, cynomolgus ES cells are more similar to human than mouse ES cells despite that ERas is expressed in cynomolgus and mouse ES cells but not in human ES cells.

Key words: Embryonic stem cell; ERas; Cynomolgus monkey; Tumorigenesis

INTRODUCTION

The ERas gene promotes the growth of and formation of teratomas by mouse ES cells by producing a constitutively active ERas protein and is not expressed in mouse ES cell-derived differentiated progeny or mouse tissues (22). Disruption of the ERas gene in mouse ES cells by homologous recombination results in a significantly reduced proliferation rate and a reduced tumorigenic potential without loss of pluripotency (22). Although the ERas gene is expressed in divergent species such as mice, dogs, and cows, it is not expressed in humans (1,12,17). Its inactivation is likely a relatively recent event in mammalian evolution. It is intriguing to speculate that some of the differences in the proliferation rate or other properties of mouse and human ES cells (9,13) are related to the differences in expression of this constitutively active ERas gene. It may also imply that the behavior of transplanted mouse ES cells does not accurately reflect the behavior of transplanted human ES cells and that the use of nonhuman primate models (11,21,25) would be more appropriate to demonstrate the safety (tumorigenicity) of human ES cell-based therapies (12). However, the expression of the ERas gene has not been examined in nonhuman primate ES cells (19,24). Here, we show that the ERas gene is expressed

Received July 18, 2008; final acceptance October 21, 2008. Online prepub date: April 15, 2009.
[1]Equal contribution.
Address correspondence to Yutaka Hanazono, M.D., Ph.D., Professor, Division of Regenerative Medicine, Center for Molecular Medicine, Jichi Medical University, 3311-1 Yakushiji, Shimotsuke, Tochigi 329-0498, Japan. Tel: +81-285-58-7451; Fax: +81-285-44-5205; E-mail: hanazono@jichi.ac.jp

in cynomolgus ES cells unlike human ES cells. In addition, the ERas gene is widely expressed in adult cynomolgus tissues. However, its forced expression in cynomolgus cells even at high levels was not related to tumorigenesis. Therefore, cynomolgus ES cells are more similar to human than mouse ES cells despite that ERas is expressed in cynomolgus and mouse ES cells but not in human ES cells.

MATERIALS AND METHODS

Cell Culture and Differentiation

A cynomolgus ES cell line (CMK6) (19), its subline (CMK6G) stably expressing enhanced green fluorescent protein (EGFP) (20), and a human ES cell line (SA181, Cellartis AB, Göteborg, Sweden) (10) were maintained on a feeder layer of mitomycin C (Kyowa, Tokyo, Japan)-treated mouse (BALB/c, Clea, Tokyo, Japan) embryonic fibroblasts (MEFs) as previously described (10,19). Confluent ES cells were dissociated from the feeder layer using 0.1% collagenase type IV (Invitrogen, Carlsbad, CA, USA). Cynomolgus stromal cells were obtained from cultured adherent cells of cynomolgus bone marrow.

For neural differentiation from cynomolgus ES cells, astrocyte-conditioned medium (ACM) was prepared by culturing astrocytes obtained from mouse fetal cerebra in Dulbecco's modified Eagle's medium (DMEM)/F12 medium containing an N2 supplement (Invitrogen) (15). Colonies of cynomolgus ES cells (800–1000 μm in diameter) were plucked from the feeder layer using a glass capillary and transferred into nonadhesive bacteriological dishes each containing ACM supplemented with 20 ng/ml of recombinant human fibroblast growth factor-2 (FGF-2) (R&D, Minneapolis, MN, USA). The colonies were cultured for 12 days, giving rise to neural stem cells, which were plated onto poly-L-lysine/laminin (Sigma-Aldrich, St. Louis, MO, USA)-coated dishes and cultivated for 7 days in Neurobasal medium supplemented with 2% B-27 (both from Invitrogen), 20 ng/ml of FGF-2, and 20 ng/ml of recombinant human epidermal growth factor (R&D). After the medium was replaced with ACM and 14 days of culture, the neural stem cells differentiated into neurons (16).

ERas Cloning and Transfection

Based on the human ERas cDNA sequence in Genbank (accession No. NM 181532), the primer set 5′-CAT GGA GCT GCC AAC AAA GCC TG-3′ and 5′-TGT GTC CCT CAA AGC TAG TTG CCT-3′ was designed for the cynomolgus ERas' complete coding sequence. Total RNA was extracted from cynomolgus ES cells using the EZ1 RNA universal tissue kit (Qiagen, Hilden, Germany) with RNase-Free DNase Set (Qiagen), and reverse-transcribed using the RNA LA PCR kit (Takara, Shiga, Japan) with an oligo dT primer. The resulting cDNA was subjected to PCR with this primer set. The PCR product was sequenced with the ABI Prism 310 (Applied Biosystems, Foster, CA, USA). The sequence analysis was performed with Genetyx-Mac software (Genetyx Corporation, Tokyo, Japan). We previously constructed the plasmids pPyCAG-EGFP-gw-IP (expressing EGFP) and pPyCAG-EGFP-gw-IP-mouse ERas (expressing EGFP-mERas) (22). The cDNA encoding the human or cynomolgus ERas gene was inserted into pPyCAG-EGFP-gw-IP to construct pPyCAG-EGFP-gw-IP-human ERas (expressing EGFP-human ERas) or pPyCAG-EGFP-gw-IP-cynomolgus ERas (expressing EGFP-cynomolgus ERas), respectively. The insert was confirmed by DNA sequencing. The plasmids were transfected into cynomolgus stromal cells using Lipofectamin 2000 (Invitrogen). The transfected cells were selected in the presence of puromycin (5 μg/ml).

Transplantation

Cells (1×10^7/site) were transplanted into the thigh muscle of immunodeficient NOD/Shi-*scid*, IL-2Rγ^{null} (NOG) mice which were purchased from Central Institute for Experimental Animals (Kanagawa, Japan). Cynomolgus ES cell-derived teratomas were generated after in utero transplantation of cynomolgus ES cells into fetal sheep as described previously (23). Adherent cells from the teratomas were propagated in DMEM (Sigma-Aldrich) supplemented with 10% fetal bovine serum (FBS) (HyClone, Logan, UT, USA). All experiments were performed in accordance with the Jichi Medical University Guide for Laboratory Animals. Experimental procedures were approved by the Animal Care and Use Committee of Jichi Medical University.

Reverse Transcription (RT)-PCR

cDNA was prepared from each sample as mentioned above and subjected to PCR with the following primer sets: for Oct-4, 5′-GGA CAC CTG GCT TCG GAT T-3′ and 5′-TTC GCT TTC TCT TTC GGG C-3′; and for glyceraldehyde-3-phosphate dehydrogenase (GAPDH), 5′-CCC TGG CCA AGG TCA TCC ATG ACA AC-3′ and 5′-CCA GTG AGC TTC CCG TTC AG-3′. Amplification conditions were 30 cycles of 95°C for 60 s, 58°C for 60 s, and 72°C for 60 s. PCR without the initial RT was also conducted to rule out DNA contamination. For real-time quantitative RT-PCR, a QuantiTect SYBR Green PCR kit (Qiagen) and the ABI Prism 7000 (Applied Biosystems) were used, and amplification conditions were 40 cycles of 95°C for 60 s, 58°C for 60 s, and 72°C for 60 s. The gene expression levels were adjusted based on those of the internal control GAPDH.

Immunoblotting

Preparation of cell lysates and Western blot analyses were performed as described previously (22). Briefly, cells (1×10^7) were washed twice with ice-cold phosphate-buffered saline (PBS) and suspended in the buffer containing 10 mM Tris-HCl (pH 7.5), 1 mM $MgCl_2$, and the 1× Complete Protease Inhibitors (Roche, Basel, Switzerland), followed by incubation on ice for 30 min. These samples were disrupted with Dounce tissue homogenizer (Wheaton, NJ, USA) and added with 1 M NaCl to a final concentration of 150 mM. For lysis, these samples were added with a final concentration of 5% SDS, 1% NP-40, and 1% deoxicorate acids, followed by incubation on ice for 10 min. The samples were then centrifuged at $12,000 \times g$ for 30 min at 4°C, and supernatants were collected. The protein concentrations were measured by the Bio-Rad Bradford assay (BioRad Laboratories, CA, USA). An equal amount of protein (10 μg per lane) was electrophoresed on 12.5% polyacrylamide gel (Atto, Tokyo, Japan) and blotted onto a PVDF membrane (Immobiron; Millipore, MA, USA). The membrane was blocked by TBST containing 5% w/v Amersham ECL-Blocking Agent (GE Healthcare, Buckinghamshire, UK) and then incubated with rabbit antiserum against mouse ERas (22) overnight at 4°C. After washed with TBST, the membrane was incubated with anti-rabbit IgG HRP (Jackson Laboratory, CA, USA) at room temperature for 60 min. Signal was detected using Amersham ECL Plus Western Blotting Detection reagents (GE Healthcare) according to the manufacturer's protocol and visualized on the LAS 3000 mini (Fujifilm, Tokyo, Japan).

Immunohistochemistry

For the immunofluorescent staining of frozen sections, tissues were fixed with 4% paraformaldehyde. The sections were labeled with rabbit anti-serum against mouse ERas (22). The primary antibody (Ab) was detected with a Tyramide Signal Amplification Kit (Invitrogen). After nuclei were stained with DAPI (Donjindo, Kumamoto, Japan), the sections were observed with a confocal laser scanning microscope (Olympus, Tokyo, Japan). For immunohistochemistry, tissues were fixed with 4% paraformaldehyde and embedded in paraffin. To identify GFP-positive cells, the sections were stained with rabbit anti-GFP Ab (Clontech, Palo Alto, CA, USA), reacted with the Dako EnVision+ System HRP (Dako, Copenhagen, Denmark), and visualized with 3,3′-diaminobenzide tetrahydrochloride (Dojindo). Nuclei were counterstained with hematoxylin.

Flow Cytometry

The expression of GFP and ERas was analyzed using a FACS Calibur flow cytometer (BD Pharmingen, San Diego, CA, USA). To detect ERas, cells were fixed using fixation/permeabilization buffer (eBioscience, San Diego, CA, USA) for 2 h at 4°C and then incubated with Alexa Fluor 647 (Invitrogen)-conjugated rabbit antiserum against ERas for 60 min at 4°C. Data acquisition and analysis were performed using CellQuest software (BD Pharmingen). Fluorescence-conjugated, irrelevant Abs served as negative controls.

Cell Proliferation Assay

Total cell numbers and proliferating cell numbers were measured with Cell Counting Kit-8 (Dojindo) and with Cell Proliferation ELISA, BrdU (colorimetric) (Roche), respectively. For Cell Counting Kit-8, cells were seeded in 96-well plates at 5×10^3 per well and measured after 6, 24, 36, 48, and 80 h of incubation according to the manufacturer's instructions. For Cell Proliferation ELISA, cells were seeded in 96-well plates at 2×10^3 per well and measured after 24, 36, 48, 72, and 96 h of incubation. Significant differences were examined using the *t*-test.

RESULTS AND DISCUSSION

Cynomolgus Cells and Tissues Express ERas

We first cloned and sequenced the cynomolgus orthologue of the ERas gene from cDNA of the undifferentiated cynomolgus ES cells (Fig. 1A). The translated amino acid sequence showed a higher degree of homology to human than mouse ERas (99% vs. 75%) (Fig. 1B). We could not detect the ERas protein in cynomolgus ES cells by flow cytometry, implying its weak expression (data not shown).

Next, we examined the expression of the ERas gene in adult cynomolgus tissues by RT-PCR. Using a primer set to cover the entire coding region, the amplicons from all nine somatic tissues were the same size as that from cynomolgus ES cells (Fig. 2A). The PCR product was sequenced to confirm that it was the ERas gene. This clearly shows that a full-length version of the ERas gene is transcribed in cynomolgus tissues, despite that ERas is not expressed in mouse tissues (22).

We then examined the protein expression in adult cynomolgus tissues by immunohistochemistry. Immunoblotting revealed that the antibody reacts to human and cynomolgus ERas as well as mouse ERas, although the antibody was generated against recombinant mouse ERas (22) (Fig. 2B). In addition, it specifically reacts to ERas (25 kDa) and does not react to other Ras family proteins (N-, H-, or K-Ras; 21 kDa) in cynomolgus cells expressing these Ras genes (Fig. 2B). Using this antibody, we detected ERas-positive cells in all tissues tested (brain, thymus, intestine, and ovary) (Fig. 2C). At a higher magnification, it turned out that ERas is localized on the cytoplasmic membrane as expected (Fig.

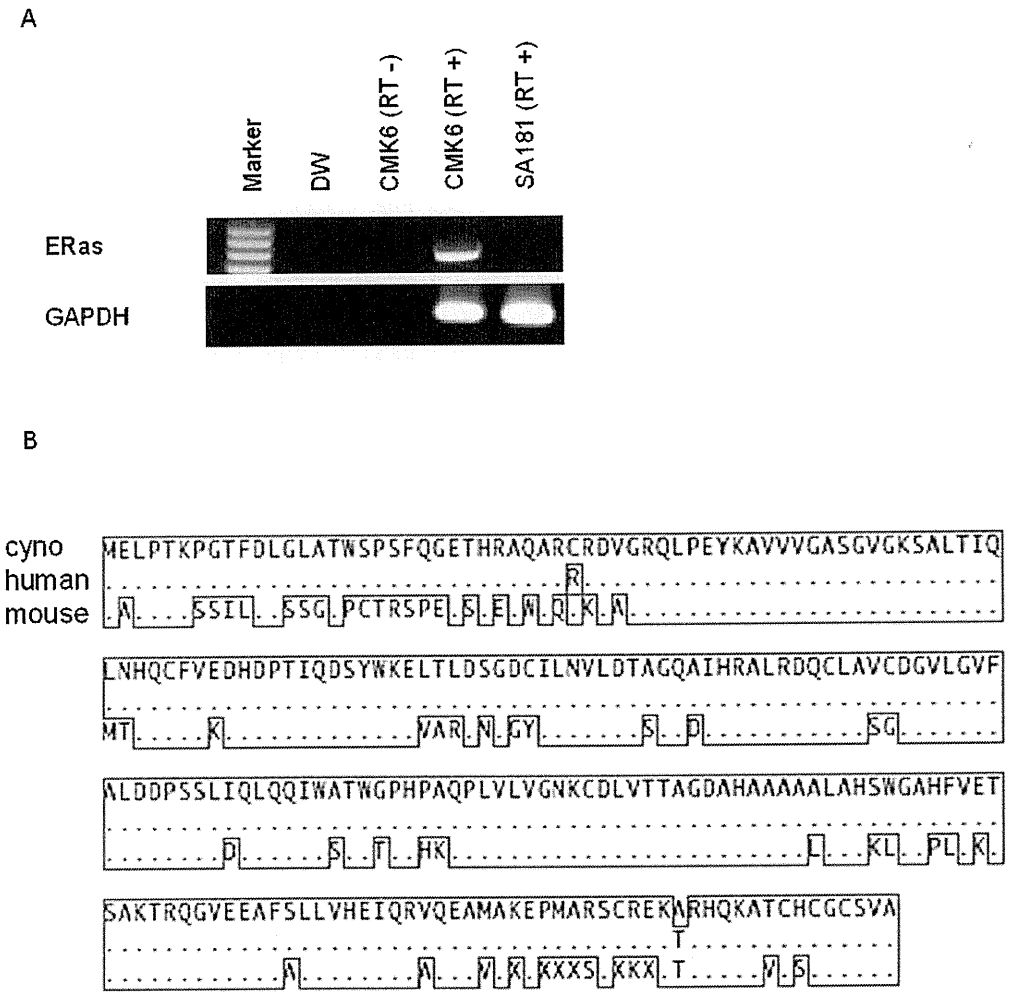

Figure 1. Cloning and sequencing of cynomolgus ERas. (A) The expression of the cynomolgus (cyno) ERas gene is detectable in cynomolgus ES cells (CMK6), but not in human ES cells (SA181), by reverse transcription (RT)-PCR. To exclude the possibility of genomic DNA contamination, PCR without the RT procedure (designated RT –) was also conducted. DW (distilled water) indicates no template in the reaction. RT-PCR of the GAPDH sequence is also shown as an internal control. (B) Amino acid sequences of cynomolgus, human (accession No. NM 181532), and mouse (accession No. NM 181548) ERas are shown. Amino acids identical to cynomolgus ERas are shown as dots and conserved amino acids are encircled with a solid line.

2D). We also tested mouse tissues, but ERas-positive cells were not detectable (Fig. 2C). Taken together, the ERas protein is indeed expressed in cynomolgus tissues, unlike in murine tissues.

The expression of the ERas gene becomes undetectable after the differentiation of mouse ES cells (22). We examined the expression of the ERas gene after the differentiation of cynomolgus ES cells. Cynomolgus ES cell-derived neurons and teratoma cells were examined for the expression of ERas as well as Oct-4, a pluripotent marker of ES cells. They were positive for ERas but negative for Oct-4 (Fig. 3A). Although cynomolgus ES cell-derived neurons were fragile and scarcely survived after dissociation from the culture dish, adherent teratoma cells could be cultured for more than six passages at a dilution of 1:4 to 1:8. Quantitative RT-PCR showed that the ERas gene expression levels were even higher in the cultured teratoma cells than in the undifferentiated cynomolgus ES cells (Fig. 3B). Then, we transplanted 1×10^7 cultured teratoma cells expressing the ERas gene (GFP-positive, passage 3) into the thigh muscle of NOG mice ($n = 3$), and examined the tumorigenicity of the cells. NOG mice were used as recipients, because they are more immunodeficient than other immunodeficient mice and transplanting to NOG mice is the most sensitive assay to detect tumorigenesis (7,14). However, no tumor developed after 2.5 months, although the transplanted cell progeny (GFP positive) were detected in every specimen (Fig. 3C). On the other hand, undifferentiated cynomolgus ES cells formed tera-

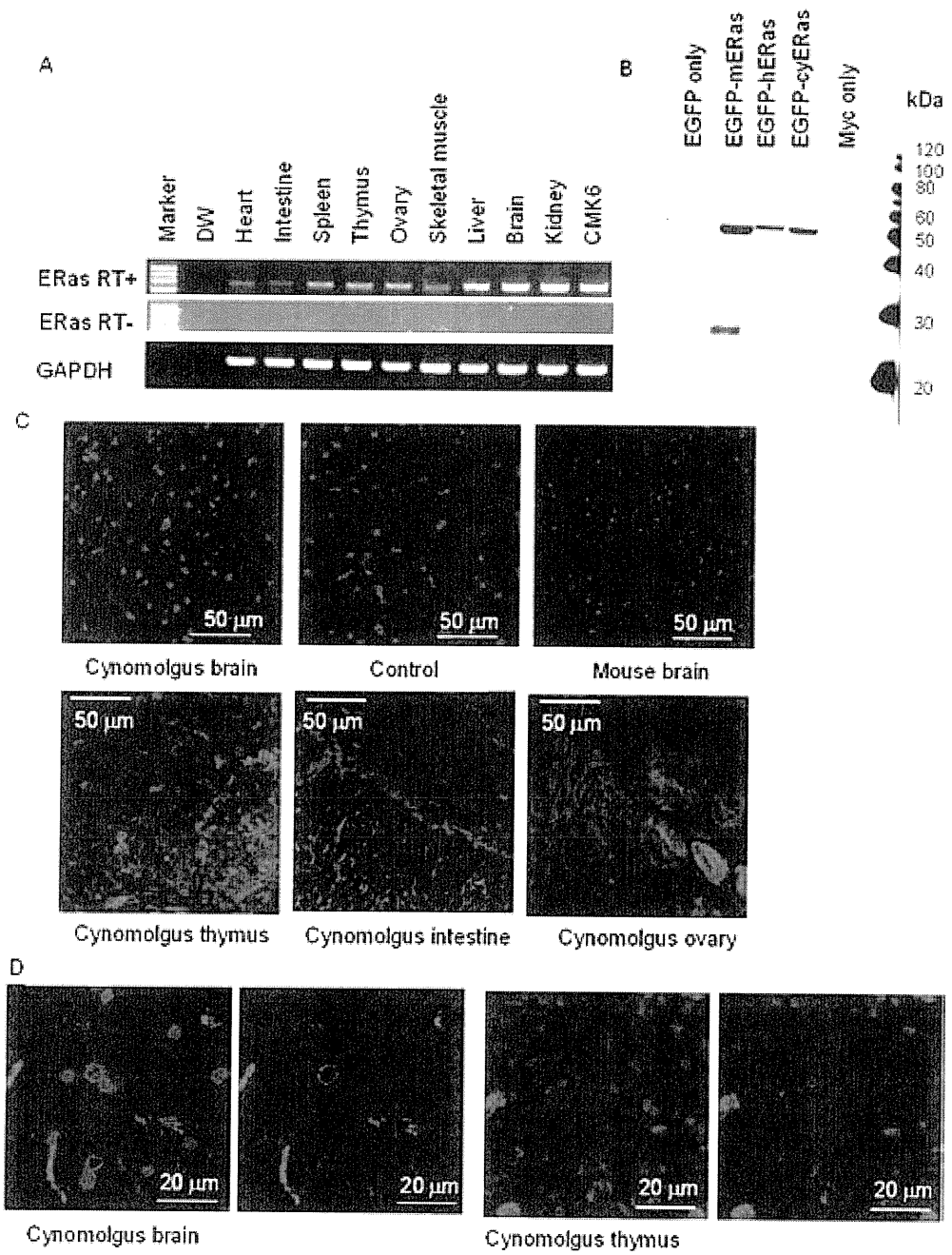

Figure 2. Cynomolgus tissues express ERas. (A) The expression of the cynomolgus ERas gene is detectable in various cynomolgus tissues by RT-PCR. To exclude the possibility of genomic DNA contamination, PCR without the RT procedure (designated RT –) was also conducted. DW indicates no template in the reaction. RT-PCR of the GAPDH sequence is also shown as an internal control. (B) Cynomolgus bone marrow stromal cells were transfected with the mouse ERas (mERas), human ERas (hERas), or cynomogus ERas (cyERas) gene fused with the EGFP gene, and immnunoblotted with the polyconal anti-ERas antibody. Although the antibody was generated against recombinant mERas (22), it reacts to hERas and cyERas as well as mERas. In addition, it does not react to cynomolgus other Ras family proteins (N-, H-, or K-Ras; 21 kDa). ERas (25 kDa) fused with EGFP (26 kDa) is detectable at 51 kDa. In mERas-transfected cells, ERas alone released from the fusion protein was also detected. (C) Using the anti-ERas antibody, ERas-positive cells (red) were detected in cynomolgus brain, thymus, intestine, and ovary. Control indicates the staining of cynomolgus brain without the primary ERas antibody. Although the primary antibody to ERas was originally developed for mouse ERas and should react more strongly to mouse than cynomolgus ERas, no positive signals were detected in mouse brain. (D) The ERas fluorescence with or without DAPI is shown at a higher magnification of both cynomolgus brain and thymus. ERas was detected on the cytoplasmic membrane.

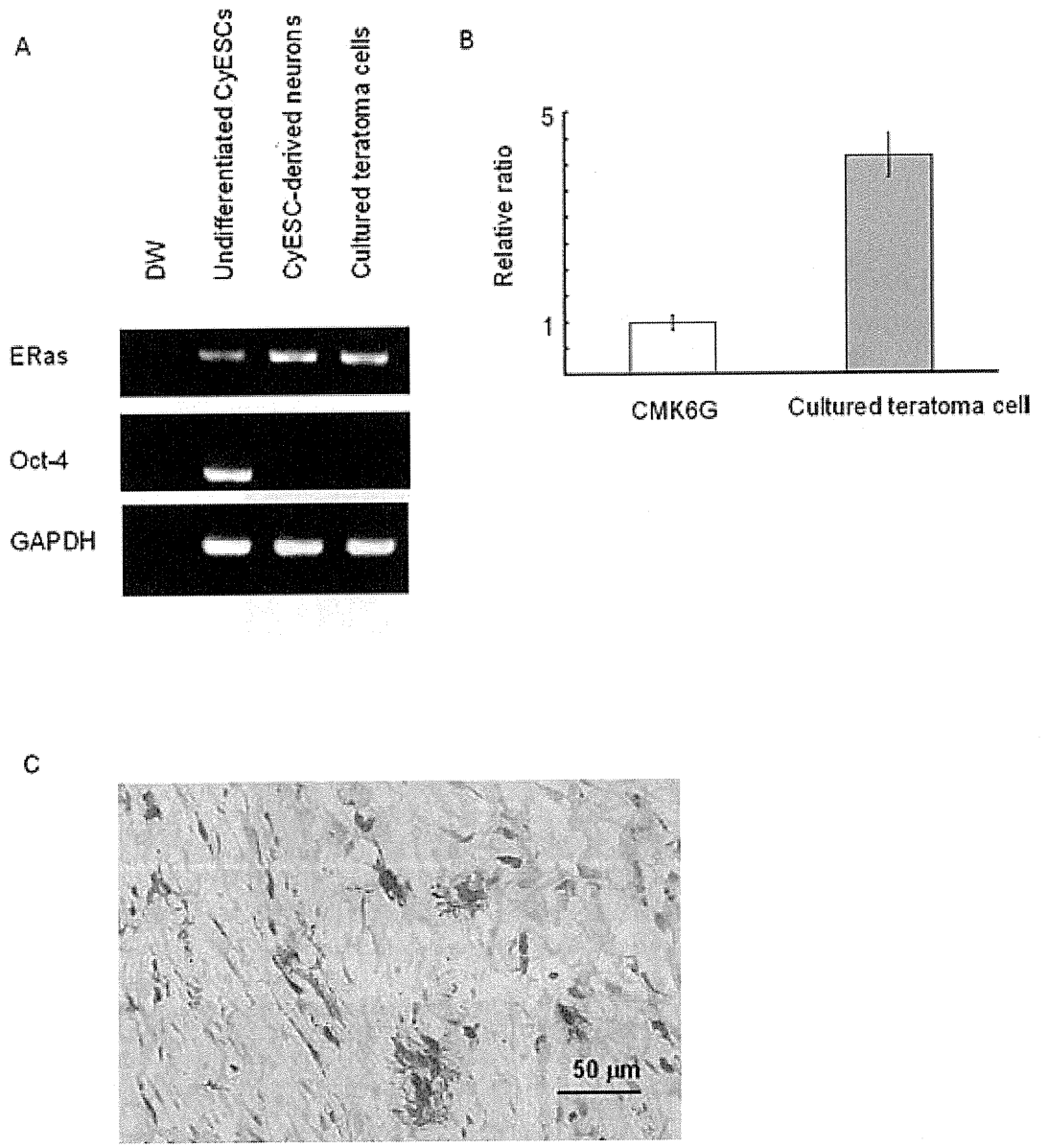

Figure 3. Cynomolgus ES cell-derived cells express ERas but do not form tumors in vivo. (A) The ERas gene was expressed in cynomolgus ES cell-derived neurons and teratoma cells as assessed by RT-PCR, whereas the Oct-4 gene was expressed in neither. DW indicates no template in the reaction. RT-PCR of the GAPDH sequence is also shown as an internal control. (B) The ERas gene expression level was nearly five times higher in the cultured teratoma cells than in the undifferentiated cynomolgus ES cells as assessed by quantitative RT-PCR. The gene expression level was adjusted using the internal control GAPDH. (C) The cultured teratoma cells were transplanted into the thigh muscles of NOG mice and examined for tumorigenicity in vivo after 2.5 months. Staining of the specimen with anti-GFP is shown. Although the transplanted cell progeny (GFP positive, brown) were detected, no tumor was observed.

tomas in all NOG mice. Taken together, cynomolgus ES cell-derived differentiated progeny and teratoma cells also express the ERas gene, but do not produce tumors in vivo.

ERas Overexpression in Cynomolgus Cells

To examine whether the cynomolgus ERas contributes to cell proliferation, we transfected cynomolgus stromal cells with a plamid expressing the cynomolgus or mouse ERas, EGFP, and puromycin resistance genes. Transfectants were obtained by treatment with puromycin and more than 90% of the cells expressed EGFP (Fig. 4A). These transfectants did not show significant morphological changes. Quantitative RT-PCR showed that the transfected cells expressed approximately 1000 times more ERas than undifferentiated cynomolgus ES

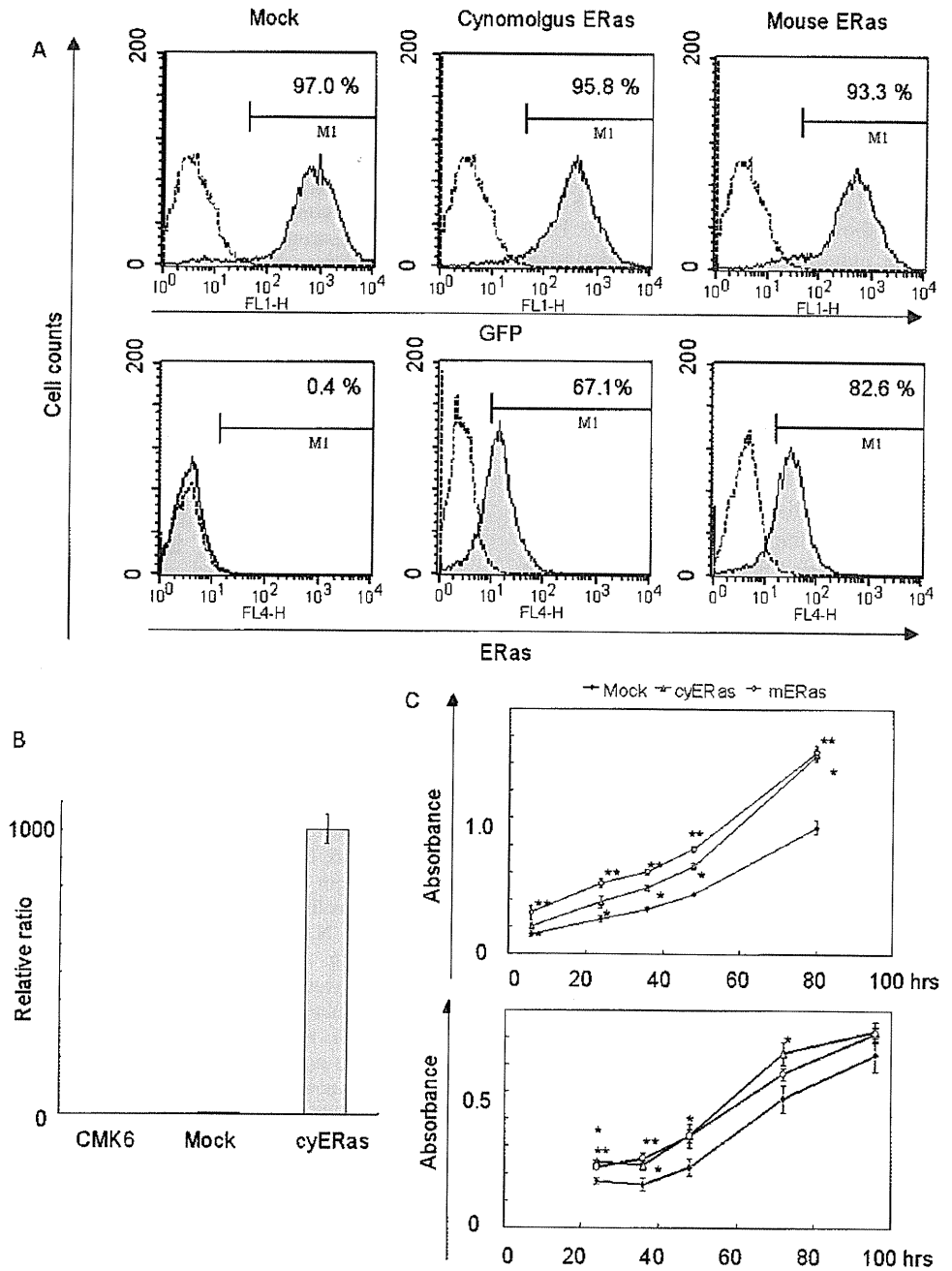

Figure 4. Overexpression of ERas does not promote cell proliferation but improves plating efficiency. (A) The plasmids expressing the cynomolgus or mouse ERas, EGFP, and puromycin resistance genes were transfected into cynomolgus stromal cells. After puromycin selection, more than 90% of cells expressed EGFP (upper). The ERas expression was also detected by flow cytometry (lower). (B) The level of cynomolgus ERas gene expression was 1000 times higher in the cynomolgus ERas-transfected cells (cyERas) than in naive cynomolgus ES cells (CMK6) or mock-transfected cells by quantitative RT-PCR. The gene expression levels were adjusted using the internal control GAPDH. (C) The mock-, cynomolgus ERas (cyERas)-, and mouse ERas (mERas)-transfected cells were plated at 5×10^3 per well and total cell numbers were measured after 6, 24, 36, 48, and 80 h of incubation (upper). The mock-, cyERas-, and mERas-transfected cells were plated at 2×10^3 per well and proliferating cell numbers were measured after 24, 36, 48, 72, and 96 h of incubation (lower). The cyERas- and mERas-transfected cells showed larger total cell or proliferating cell numbers after plating than the mock-transfected cells, but did not show any more rapid proliferation thereafter. Statistical differences with the *t*-test are indicated: $*p < 0.01$ for the cyERas- versus mock-transfected cells, $**p < 0.01$ for the mERas- versus mock-transfected cells.

cells (Fig. 4B). These cells expressing either cynomolgus or mouse ERas showed larger total cell numbers or proliferating cell numbers after plating than the mock-transfected cells, but did not show any more rapid proliferation thereafter (Fig. 4C). Thus, cynomolgus ERas improves plating efficiency but does not promote cell proliferation, even when it is expressed at high levels.

In this report, we showed that the cynomolgus ERas gene is expressed in cynomolgus ES cells and tissues. Its expression pattern is quite different from that of mouse ERas, which is not expressed in mouse ES cell-derived differentiated progeny or mouse tissues. Although cynomolgus ERas improved the plating efficiency when overexpressed, its expression did not promote cell proliferation or induce tumor formation in vivo (Figs. 3C, 4C). Thus, cynomolgus ERas might only suppress the apoptosis of cynomolgus cells (5). Because the formation of teratomas is one of the greatest obstacles to the clinical application of human ES cells (3,8,18), it is important to elucidate whether the ERas gene expressed in cynomolgus ES cells is related to teratoma development in vivo in order to tell whether nonhuman primate models are really suitable for preclinical research. From our study, it is at least suggested that cynomolgus ES cells are more similar to human than mouse ES cells in that ERas does not contribute to the formation of teratomas in vivo.

To date, the pluripotent marker Oct-4 has been used to predict the formation of teratomas (4) and the removal of Oct-4-positive cells from ES cell-derived progenitor preparations is reported to prevent teratomas from developing posttransplant (2). However, Oct-4-negative immature cells are also reported to contribute to the formation of teratomas (6). Therefore, although Oct-4 could be used to predict whether teratomas develop to some extent, it does not regulate the developmental process. For future clinical applications, the mechanism by which primate ES cells form teratomas should be studied in more detail.

ACKNOWLEDGMENTS: We thank Naomi Takino for technical assistance and Shuh-hei Fujishiro for helpful discussion. This study was supported by grants (JMS 21st Century COE Program, High-tech Research Center Program, and KAKENHI) from the Ministry of Education, Culture, Sports, Science and Technology of Japan as well as grants (KAKENHI) from the Ministry of Health, Labor and Welfare of Japan.

REFERENCES

1. Bhattacharya, B.; Miura, T.; Brandenberger, R.; Mejido, J.; Luo, Y.; Yang, A. X.; Joshi, B. H.; Ginis, I.; Thies, R. S.; Amit, M.; Lyons, I.; Condie, B. G.; Itskovitz-Eldor, J.; Rao, M. S.; Puri, R. K. Gene expression in human embryonic stem cell lines: unique molecular signature. Blood 103:2956–2964; 2004.
2. Bieberich, E.; Silva, J.; Wang, G.; Krishnamurthy, K.; Condie, B. G. Selective apoptosis of pluripotent mouse and human stem cells by novel ceramide analogues prevents teratoma formation and enriches for neural precursors in ES cell-derived neural transplants. J. Cell Biol. 167:723–734; 2004.
3. Bjorklund, L. M.; Sanchez-Pernaute, R.; Chung, S.; Andersson, T.; Chen, I. Y.; McNaught, K. S.; Brownell, A. L.; Jenkins, B. G.; Wahlestedt, C.; Kim, K. S.; Isacson, O. Embryonic stem cells develop into functional dopaminergic neurons after transplantation in a Parkinson rat model. Proc. Natl. Acad. Sci. USA 99:2344–2349; 2002.
4. Campbell, P. A.; Perez-Iratxeta, C.; Andrade-Navarro, M. A.; Rudnicki, M. A. Oct4 targets regulatory nodes to modulate stem cell function. PLoS ONE 2:e553; 2007.
5. Cox, A. D.; Der, C. J. The dark side of Ras: Regulation of apoptosis. Oncogene 22:8999–9006; 2003.
6. Dihne, M.; Bernreuther, C.; Hagel, C.; Wesche, K. O.; Schachner, M. Embryonic stem cell-derived neuronally committed precursor cells with reduced teratoma formation after transplantation into the lesioned adult mouse brain. Stem Cells 24:1458–1466; 2006.
7. Erdo, F.; Buhrle, C.; Blunk, J.; Hoehn, M.; Xia, Y.; Fleischmann, B.; Focking, M.; Kustermann, E.; Kolossov, E.; Hescheler, J.; Hossmann, K. A.; Trapp, T. Host-dependent tumorigenesis of embryonic stem cell transplantation in experimental stroke. J. Cereb. Blood Flow Metab. 23: 780–785; 2003.
8. Fujikawa, T.; Oh, S. H.; Pi, L.; Hatch, H. M.; Shupe, T.; Petersen, B. E. Teratoma formation leads to failure of treatment for type I diabetes using embryonic stem cell-derived insulin-producing cells. Am. J. Pathol. 166:1781–1791; 2005.
9. Hasegawa, K.; Fujioka, T.; Nakamura, Y.; Nakatsuji, N.; Suemori, H. A method for the selection of human embryonic stem cell sublines with high replating efficiency after single-cell dissociation. Stem Cells 24:2649–2660; 2006.
10. Heins, N.; Englund, M. C.; Sjoblom, C.; Dahl, U.; Tonning, A.; Bergh, C.; Lindahl, A.; Hanson, C.; Semb, H. Derivation, characterization, and differentiation of human embryonic stem cells. Stem Cells 22:367–376; 2004.
11. Hematti, P.; Obrtlikova, P.; Kaufman, D. S. Nonhuman primate embryonic stem cells as a preclinical model for hematopoietic and vascular repair. Exp. Hematol. 33:980–986; 2005.
12. Kameda, T.; Thomson, J. A. Human ERas gene has an upstream premature polyadenylation signal that results in a truncated, noncoding transcript. Stem Cells 23:1535–1540; 2005.
13. Kaufman, D. S.; Thomson, J. A. Human ES cells—haematopoiesis and transplantation strategies. J. Anat. 200: 243–248; 2002.
14. Kishi, Y.; Tanaka, Y.; Shibata, H.; Nakamura, S.; Takeuchi, K.; Masuda, S.; Ikeda, T.; Muramatsu, S.; Hanazono, Y. Variation in the incidence of teratomas after transplantation of nonhuman primate ES cells into immunodeficient mice. Cell Transplant. 17(9):1095–1102; 2008.
15. Nakayama, T.; Momoki-Soga, T.; Inoue, N. Astrocyte-derived factors instruct differentiation of embryonic stem cells into neurons. Neurosci. Res. 46:241–249; 2003.
16. Nakayama, T.; Momoki-Soga, T.; Yamaguchi, K.; Inoue, N. Efficient production of neural stem cells and neurons from embryonic stem cells. Neuroreport 15:487–491; 2004.
17. Rao, M. Conserved and divergent paths that regulate self-

renewal in mouse and human embryonic stem cells. Dev. Biol. 275:269–286; 2004.
18. Shibata, H.; Ageyama, N.; Tanaka, Y.; Kishi, Y.; Sasaki, K.; Nakamura, S.; Muramatsu, S.; Hayashi, S.; Kitano, Y.; Terao, K.; Hanazono, Y. Improved safety of hematopoietic transplantation with monkey embryonic stem cells in the allogeneic setting. Stem Cells 24:1450–1457; 2006.
19. Suemori, H.; Tada, T.; Torii, R.; Hosoi, Y.; Kobayashi, K.; Imahie, H.; Kondo, Y.; Iritani, A.; Nakatsuji, N. Establishment of embryonic stem cell lines from cynomolgus monkey blastocysts produced by IVF or ICSI. Dev. Dyn. 222:273–279; 2001.
20. Takada, T.; Suzuki, Y.; Kondo, Y.; Kadota, N.; Kobayashi, K.; Nito, S.; Kimura, H.; Torii, R. Monkey embryonic stem cell lines expressing green fluorescent protein. Cell Transplant. 11:631–635; 2002.
21. Takagi, Y.; Takahashi, J.; Saiki, H.; Morizane, A.; Hayashi, T.; Kishi, Y.; Fukuda, H.; Okamoto, Y.; Koyanagi, M.; Ideguchi, M.; Hayashi, H.; Imazato, T.; Kawasaki, H.; Suemori, H.; Omachi, S.; Iida, H.; Itoh, N.; Nakatsuji, N.; Sasai, Y.; Hashimoto, N. Dopaminergic neurons generated from monkey embryonic stem cells function in a Parkinson primate model. J. Clin. Invest. 115:102–109; 2005.
22. Takahashi, K.; Mitsui, K.; Yamanaka, S. Role of ERas in promoting tumour-like properties in mouse embryonic stem cells. Nature 423:541–545; 2003.
23. Tanaka, Y.; Nakamura, S.; Shibata, H.; Kishi, Y.; Ikeda, T.; Masuda, S.; Sasaki, K.; Abe, T.; Hayashi, S.; Kitano, Y.; Nagao, Y.; Hanazono, Y. Sustained macroscopic engraftment of cynomolgus embryonic stem cells in xenogeneic large animals after in utero transplantation. Stem Cells Dev. 17:367–382; 2008.
24. Thomson, J. A.; Kalishman, J.; Golos, T. G.; Durning, M.; Harris, C. P.; Becker, R. A.; Hearn, J. P. Isolation of a primate embryonic stem cell line. Proc. Natl. Acad. Sci. USA 92:7844–7848; 1995.
25. Wolf, D. P. Nonhuman primate embryonic stem cells: An underutilized resource. Regen. Med. 3:129–131; 2008.